Turkish Journal of Civil Engineering, 2024 109-138, Paper 759, ***Research Article***

Behavior of Base-Isolated Liquid Storage Tanks with Viscous Dampers under Historical Earthquakes Considering Superstructure Flexibility

Elif GÜLER[1]
Cenk ALHAN[2*]

ABSTRACT

Liquid storage tanks (LSTs) can be efficiently protected from far-fault earthquakes by base-isolation. However, large isolation system and sloshing displacements may threaten the tank's safety under near-fault earthquakes. Although the application of supplemental viscous dampers (VDs) at the base-isolation systems of LSTs located in near-fault areas may help, it may also increase superstructure demands under far-fault earthquakes. In addition to the characteristics of the earthquake, the isolation system and the superstructure properties may affect the success of base-isolated LSTs with supplemental VDs. Therefore, a numerical investigation is conducted in this study in order to determine the influence of the supplemental viscous damping ratio, the isolation system period, the tank wall flexibility, and the tank slenderness ratio on the seismic responses of base-isolated cylindrical steel LSTs with supplemental VDs including the base displacement, the sloshing displacement, and the normalized isolation system shear force under both near-fault and far-fault historical earthquake records. The tank is modeled by single-degree-of-freedom systems representing different modes on a common isolation basemat and the nonlinear dynamic analyses are carried out in 3D-BASIS-ME software. Findings show that while supplemental damping is required especially when LSTs with long-period isolation systems are subjected to large magnitude near-fault earthquakes, it may also cause amplifications in the sloshing displacement and isolation system shear force demands in case of far-fault earthquakes. Furthermore, it is determined that the influence of tank flexibility on both the superstructure and the isolation system responses is negligibly small while the tank slenderness ratio may have considerable effects.

Keywords: Liquid storage tank, base-isolation, supplemental viscous damper, near-fault earthquake, parametric analysis.

Note:
- This paper was received on October 10, 2022 and accepted for publication by the Editorial Board on October 13, 2023.
- Discussions on this paper will be accepted by March 31, 2024.

• https://doi.org/10.18400/tjce.1380129

1 Maltepe University, Department of Civil Engineering, Istanbul, Türkiye
elifguler@maltepe.edu.tr - https://orcid.org/0000-0001-5261-5320

2 Istanbul University-Cerrahpaşa, Department of Civil Engineering, Istanbul, Türkiye
cenkalhan@iuc.edu.tr - https://orcid.org/0000-0002-6649-8409

* Corresponding author

1. INTRODUCTION

Along with the development of the economy and the increase in the density of the population, liquid storage tanks (LSTs) are becoming widespread and increasing in size today in order to meet the needs of the society. The exposure of these tanks to earthquakes can cause significant failures such as structural collapse, loss of function, fire, hazardous material leak, environmental pollution, and groundwater contamination which affects various sections of industry such as nuclear, chemical, pharmaceutical, food, or oil [1-3]. For example, Hatayama [4] reported that the 2003 Tokachi-oki Japan Earthquake (M_w=8.0), which produced large-amplitude and long-period (4-8 s) ground motions, caused severe damage in the seven large oil storage tanks with floating roof structures, leading to dangerous situations such as ring fire, roof sinking, and open-top fire because of severe sloshing of oil. Yazici and Cili [5] mentioned that the 1999 Kocaeli Turkey Earthquake caused fires in the Tüpraş İzmit Refinery, damaging more than 30 floating-roof naphtha tanks and at the Habas plant, 2 elevated liquid oxygen tanks collapsed because of the detrimental effects of the earthquake on the reinforced concrete pedestal.

In recent years, employing base-isolation is suggested as an effective way for the earthquake-resistant design of the LSTs. There are many studies in the literature showing the effect of base-isolation on the seismic responses of LSTs from different perspectives. Jadhav and Jangid [6] compared the responses of LSTs isolated by laminated rubber bearings, lead-rubber bearings, and friction pendulum systems with those of non-isolated systems under real earthquake ground motions considering the effects of parameters such as the aspect ratio of the tank and the isolation period. They stated that the elastomeric bearings with lead cores exhibited the best performance. Furthermore, they demonstrated that the proposed approximate model for evaluating seismic responses provided satisfactory estimations. Shrimali and Jangid [7] concluded that the effects of non-classical damping are generally insignificant and the responses obtained through modal analysis using the classical damping approach can be accurately calculated. Additionally, their analyses conducted using the response spectrum method and a simplified approximate method proposed showed that the responses obtained are consistent with the exact responses. In their study, Jadhav and Jangid [8] subjected LSTs isolated with elastomeric bearings and sliding systems to the fault normal and parallel components of near-fault ground motions. They demonstrated that the fault normal component mainly governs the resultant response. Additionally, they examined the effects of parameters such as the aspect ratio of the tank, isolation period, and damping of the isolation bearings on the effectiveness of seismic isolation. They emphasized that increasing the damping beyond the optimum value may result in an increase in base shear. Shekari et al. [9] examined the behavior of cylindrical LSTs modeled using finite shell elements and boundary elements combined with base isolation systems consisting of bilinear hysteretic bearing elements under long-period ground motions. Through their analysis using an iterative and step-by-step algorithm, they found that significant reduction in dynamic responses may be achieved with such isolation systems. Panchal and Soni [10] evaluated the studies in the literature about the behavior of seismically isolated liquid storage tanks with various shapes and materials under seismic excitations. They noted that most studies have shown that isolating liquid storage tanks effectively reduces the impulsive response component while causing a small increase in the convective component but the studies are still insufficient on some subjects. They have suggested examples of topics that require further research in the future, such as investigating the impact of three-axis earthquake

excitation on the responses of isolated steel tanks containing multilayered liquid, analyzing and assessing the feasibility of semi-active control devices for the aseismic design of fluid storage ground and elevated steel tanks. Saha et al. [11] modeled the base-isolated cylindrical steel water storage tanks with the Response Surface Model in order to investigate the effect of the uncertainty in the mechanical parameters of lead rubber bearings on the peak seismic responses using fragility curves obtained via Monte Carlo simulation. They found that such uncertainties affect the peak response quantities and the probability of failure for the base-isolated liquid storage tanks reduces as the isolation period increases. Hashemi and Aghashiri [12] conducted seismic analyses of base-isolated flexible rectangular fluid containers made of concrete under horizontal ground motion using an equivalent mechanical model. They concluded that the base shear, wall deformation, and hydrodynamic pressure of the rectangular fluid containers could be effectively reduced by base-isolation but the surface sloshing height of the fluid in the container could be increased. Alhan et al. [13] investigated the effect of the characteristic strength ratio on the seismic response behavior of cylindrical steel LSTs seismically isolated with lead-rubber bearings under representative near-fault and far-fault earthquakes. They concluded that higher characteristic strength ratio effectively helps reducing large base displacement under near-fault earthquakes but this may have a negative impact on the superstructure responses especially under far-fault earthquakes. In their dynamic analyses considering different damping models for isolators, including interpolated damping, Rayleigh damping with override, Rayleigh damping, constant damping with override, and constant damping for all modes, Tsipianitis and Tsompanakis [14] demonstrated that the most suitable method for numerical modeling of isolator's damping for a squat cylindrical liquid storage tank isolated with single friction pendulum bearings under strong near-fault ground motions is Rayleigh damping with override. In order to enhance the dynamic performance of base-isolated cylindrical LSTs, Tsipianitis and Tsompanakis [3] used sizing optimization of the main parameters of single friction pendulum bearings and triple friction pendulum bearings via efficient swarm intelligence optimization algorithms.

It is possible to effectively benefit from base-isolation systems in protecting liquid storage tanks from *far-fault* earthquakes with high-frequency content. However, when *near-fault* earthquakes are considered, large-amplitude velocity pulses with long periods, which are generally in the range of 2 s ~ 4 s [15-19], may coincide with the isolation periods of the base-isolated LSTs, which are generally in the range of 2 s ~ 4 s, and result in very large isolation system displacements that directly threaten the tank safety [20-22]. Dynamic behavior of liquid storage tanks is represented by the combination of three main modes, namely the sloshing/convective mode, the fluid-tank mode, and the rigid impulsive mode associated with the sloshing of the fluid in the tank, the deformation of the tank wall, and the non-vibratory part of the fluid, respectively [23]. In particular, the period of the sloshing mode is typically a long one and thus may coincide with the near-fault earthquake pulse periods, resulting in very large sloshing displacements. There are various research studies in the literature about the dynamic responses of base-isolated LSTs under near-fault earthquakes. For example, Alhan et al. [22] exemplified the seismic responses of a benchmark base-isolated cylindrical LST made of steel under synthetically generated sample near-fault earthquake records of different magnitudes at different fault-distances. Kalogerakou et al. [24] examined the hydrodynamic responses of rigid cylindrical liquid storage tanks by emphasizing the near-fault phenomenon. They showed that according to the

concept presented by Housner [25] considering an impulsive and a series of convective modes, neglecting the second convective mode can have important effects in predicting the maximum shaking wave height. Öncü-Davas et al. [26] evaluated the success of synthetic earthquake records generated by using different pulse models in representing equivalent historical earthquake records in terms of the seismic responses of base-isolated steel LSTs with a circular plan. Safari and Tarinejad [27] conducted a parametric study of stochastic seismic responses of base-isolated cylindrical steel LSTs under near-fault and far-fault ground motions to evaluate the influence of characteristic parameters of the storage tanks and isolation system and excitation features. Zhao et al. [2] showed that using ADINA software is feasible to simulate the sloshing wave heights of large vertical cylindrical storage tanks made of steel under near-fault earthquakes by comparing the shaking table test results with the results from the finite element simulation. They also conducted a research on the rationality of the wave-height fortification of national storage tank specifications.

As described above, large isolation system and sloshing displacements may be observed for base-isolated LSTs located in near-fault regions. In order to tackle this near-fault earthquake challenge, supplemental viscous dampers may be employed at the base-isolation systems of LSTs located in regions close to active faults. However, there are limited studies in the literature about the seismic behavior of base-isolated LSTs equipped with supplemental viscous dampers. In a numerical example of an earlier technical report, it is demonstrated how supplemental viscous dampers can be employed at the base-isolation system of a sample cylindrical steel LST model via the 3D-BASIS-ME program [28]. The study considers a single superstructure model, with H/R and h/R ratios of 0.67 and 0.0014, respectively, and a single rubber base-isolation system consisting of low-damping rubber bearings with linear viscous fluid dampers. In an experimental study, Castellano et al. [29] presented preliminary results of the shaking table tests conducted on a cylindrical liquefied natural gas storage tank mock-up seismically protected with laminated rubber bearings and steel hysteretic torsional dampers. In a more recent conference paper, Gazi et al. [30] numerically demonstrated the potential improvement in seismic response of base-isolated steel LSTs considering a single superstructure model with a circular plan [28], only, when nonlinear supplemental viscous dampers are employed in the isolation system. And, Luo et al. [31] proposed a hybrid control system, which simultaneously adjusts mass, stiffness, and damping, consisting of a viscous mass damper used with a rubber bearing to mitigate the liquid sloshing in cylindrical storage tanks. As a predecessor of the present work, Güler and Alhan [32] evaluated the seismic responses of a single benchmark squat (H/R=0.50) tank model, only, in order to determine the performance limits of base-isolated LSTs with/without supplemental viscous damping under near-fault earthquakes using synthetically generated pulse models. Most recently, Tsipianitis and Tsompanakis [33] investigated the beneficial impact of supplemental linear viscous dampers on the seismic performance of steel LSTs with the cylindrical form equipped with single friction pendulum devices in terms of isolators' displacement capacity and superstructure accelerations under a suite consisting of twenty near-fault accelerograms. They modelled the liquid tanks utilizing the so-called "Joystick" model presented by Bakalis et al. [34] for fixed-base tanks. In order to portray a complete picture for base-isolated LSTs equipped with rubber bearings and supplemental viscous dampers, it is essential to perform a comprehensive examination considering a wide range of both *superstructure* and *isolation system* characteristic parameters (the supplemental viscous damping ratio, the isolation system period, the tank wall flexibility, and the tank slenderness ratio) under both historical

near-fault and historical *far-fault* earthquake records encompassing a wide frequency range. In this study, a parametric investigation is carried out via nonlinear seismic response analyses in order to determine the influence of the considered parameters on the base displacement, the sloshing displacement, and the isolation system shear force demands.

The assumptions and limitations of this study can be summarized as follows: simplified lumped mass model [23] is taken into account. The wave-wave, wave-wall and wave-roof interactions are neglected. Fully symmetric base-isolation systems are taken into account in order to avoid eccentricity. Unidirectional excitation is considered in the time history analysis, ignoring the effect of the vertical components of the ground motions. Finally, soil-structure interaction is not taken into account.

The outline of the content can be summarized as follows: First, the properties of the tank superstructures and the base-isolation systems consisting of isolators and supplemental viscous dampers are introduced. Then, the numerical modeling of the base-isolated LSTs with supplemental viscous dampers is described. Next, the characteristics of twelve historical earthquake records, six representing near-fault and six representing far-fault earthquakes, are presented. Then, the nonlinear time history response results are discussed in terms of both the peak and the average responses in a comparative manner as a function of the parameters including the tank flexibility, the tank slenderness ratio, the isolation system period, and the supplemental viscous damping ratio. Finally, the conclusions drawn are presented.

2. BASE-ISOLATED LST MODELS WITH SUPPLEMENTAL VISCOUS DAMPERS

Within the scope of the study conducted by Güler [35], the base-isolated LST model equipped with supplemental viscous dampers whose schematic view given in Figure 1 is used. The overall tank geometry is similar to that considered by Tsopelas et al. [28]. The tank has a cylindrical steel wall of thickness h and is covered with a concave steel roof that allows the liquid to slosh without spilling. The radius (R) of the circular tank plan is 18.29 m and the

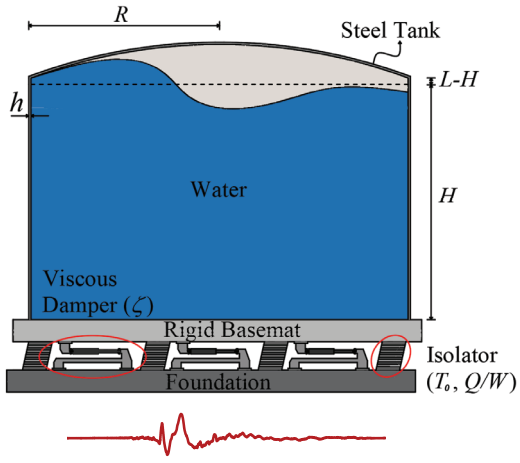

Figure 1 - Schematic view of the base-isolated LST with supplemental viscous dampers.

height of the water (H) in the tank is 0.61 m below the tank wall height (L). The tank is placed on a reinforced concrete basemat with a thickness of h_b=45.72 cm and a radius of R_b=18.59 m. In the following subsections, first, the superstructure (i.e. tank) model parameters including the ratio of the water height to the tank radius (H/R) and the ratio of the steel tank wall thickness to the tank radius (h/R) are defined. Then, isolation system model parameters (i.e. the characteristic values of the isolators and supplemental viscous dampers), including the characteristic strength of the isolation system to the total structure weight ratio (Q/W), the post-yield isolation system period (T_0), and the total supplemental viscous damping coefficient (ζ) are presented. Finally, the numerical modeling base-isolated LSTs with supplemental viscous dampers in 3D-BASIS-ME [28] software is explained. A total of 112 different models are formed by combining fourteen different superstructures with eight different base-isolation systems.

2.1. Tank Superstructure

Two main superstructure parameters that influence the seismic behavior of LSTs are (i) the ratio of water height to the tank radius (H/R) and (ii) the ratio of steel tank wall thickness to the tank radius (h/R). In this study, H/R values are chosen as 0.50, 0.75, 1.00, 1.25, 1.50, 1.75, and 2.00 in order to cover a wide practical range of slenderness ratio -from squat to slender- and h/R values are taken into account as 0.001 and 0.004, in order to consider flexible and rigid cases, respectively. The range of the selected parameters are in general compliance with those used in the literature [e.g., 27, 36-39]. Using the unit weights of 7850 kg/m^3, 1000 kg/m^3, and 2400 kg/m^3 for steel, water and concrete, respectively, the weight of water in the tank (W_w), the reinforced concrete basemat (W_{cb}), and the steel tank (W_{st}) and the total superstructure weight (W_t=W_w+W_{cb}+W_{st}) are calculated for each tank and reported in Table 1. The steel tank weight includes the weights of the tank wall and the roof.

Table 1 - Weights of LST models.

H/R	W_{st} [kN]		W_w [kN]	W_{cb} [kN]	W_t [kN]	
	h/R= 0.001	h/R= 0.004			h/R= 0.001	h/R= 0.004
0.50	3106.3	12425.1	94705.2	11699.8	109511.3	118830.1
0.75	3845.8	15383.2	142057.8	11699.8	157603.4	169140.8
1.00	4585.3	18341.3	189410.4	11699.8	205695.5	219451.5
1.25	5324.9	21299.5	236763.0	11699.8	253787.6	269762.2
1.50	6064.4	24257.6	284115.6	11699.8	301879.8	320073.0
1.75	6803.9	27215.7	331468.2	11699.8	349971.9	370383.7
2.00	7543.5	30173.8	378820.8	11699.8	398064.0	420694.4

2.2. Base-Isolation System - Isolators and Supplemental Viscous Dampers

The base-isolation system consists of 52 equivalent rubber-based isolators placed in a symmetrical fashion under the rigid reinforced concrete basemat and 24 equivalent supplemental viscous dampers placed in parallel with the isolators whose general layout is given in Figure 2 [28].

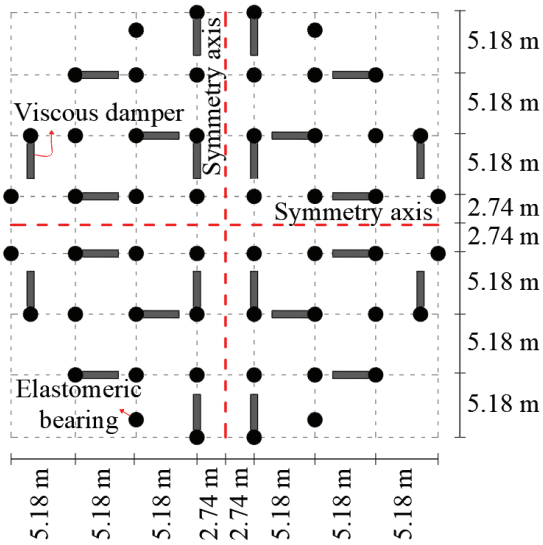

Figure 2 - Layout of the base-isolation system (modified from Tsopelas et al. [28]).

Rubber-based isolators show nonlinear hysteretic behavior. The behavior of these isolators can be represented by a smooth bilinear force (F)-displacement (D) curve [40] obtained by using an extended version of the Bouc-Wen [41, 42] hysteretic model presented by Park et al. [43] for biaxial interactions. In this regard, forces developed in the rubber-based isolators along orthogonal x and y directions are obtained by the following equations depending on the yield strength (F_y), the yield displacement (D_y), and the post-yield to pre-yield stiffness ratio (α):

$$F_x = \alpha \frac{F_y}{D_y} U_x + (1-\alpha) F_y Z_x \tag{1}$$

$$F_y = \alpha \frac{F_y}{D_y} U_y + (1-\alpha) F_y Z_y \tag{2}$$

Here, while U_x and U_y are the displacements of the rubber-based isolators in two orthogonal directions, Z_x and Z_y are the dimensionless hysteretic variables given by the following Equation [43]:

$$\begin{Bmatrix} \dot{Z}_x D_y \\ \dot{Z}_y D_y \end{Bmatrix} = \begin{Bmatrix} A\dot{U}_x \\ A\dot{U}_y \end{Bmatrix} - \begin{bmatrix} Z_x^2(\gamma \text{Sign}(\dot{U}_x Z_x) + \beta) & Z_x Z_y(\gamma \text{Sign}(\dot{U}_y Z_y) + \beta) \\ Z_x Z_y(\gamma \text{Sign}(\dot{U}_x Z_x) + \beta) & Z_y^2(\gamma \text{Sign}(\dot{U}_y Z_y) + \beta) \end{bmatrix} \begin{Bmatrix} \dot{U}_x \\ \dot{U}_y \end{Bmatrix} \tag{3}$$

where $\dot{U}_x$ and $\dot{U}_y$ are the velocities of the rubber-based isolators in two orthogonal directions, and Sign is the signum function. On the other hand, A, γ, and β are dimensionless quantities that control the shape of the hysteresis loop. And they are accepted as 1.0, 0.9, and 0.1 to represent the smooth bilinear force-displacement loop, respectively [28]. A graphical representation of the smooth bilinear force-displacement curve is given in Figure 3.

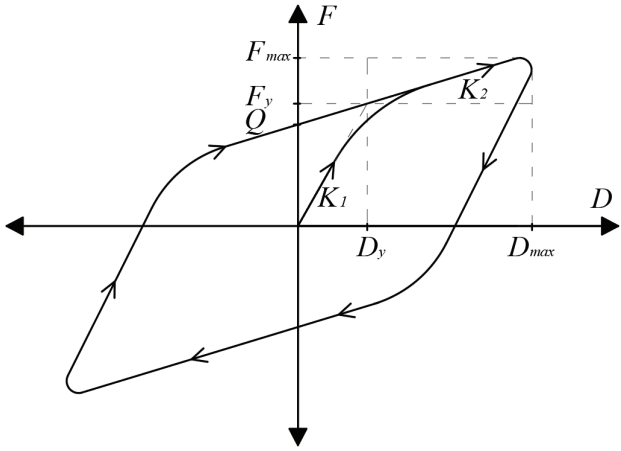

Figure 3 - Smooth bilinear force-displacement curve [44].

In this context, the basic mechanical parameters of the isolation system, which determine the seismically isolated behavior of the structure and used in 3D-BASIS-ME [28] can be listed as the pre-yield stiffness (K_1), the post-yield stiffness (K_2), the characteristic force (Q), the yield strength (F_y), and the yield displacement (D_y). For a total weight of W supported by the isolators, the post-yield isolation period (also known as rigid-body period) is presented as follows [40]:

$$T_0 = 2\pi / \sqrt{K_2 \left(g / W \right)} \tag{4}$$

The relationship between other parameters and the ratio of post-yield stiffness to pre-yield stiffness α is defined as follows [44]:

$$Q = (K_1 - K_2) \times D_y \tag{5}$$

$$K_1 = F_y / D_y \tag{6}$$

$$\alpha = K_2 / K_1 \tag{7}$$

In this study, two main sets of isolation systems with T_0=2 and 4 s that correspond to short and long-period isolation systems, respectively, are considered. The characteristic values for the isolation systems of each base-isolated LST model are obtained by using the relations presented in Equations (4), (5), (6), and (7) and given in Table 2. In calculating the isolation periods and the characteristic force ratios, the effective weight (W) values obtained by subtracting the flexible sloshing mode weight (W_s) from the total weight on the isolation system (W_t) are used, as suggested by Tsopelas et al. [28]. The characteristic strength ratio (Q/W) is assumed as 5% and the yield displacement (D_y) is accepted as 1.5 cm.

Table 2 - Characteristic values of the isolation systems.

H/R	W [kN×10^{-3}]	Q [kN×10^{-3}]	T_0=2 s, α=0.23			T_0=4 s, α=0.07		
			K_2 [kN/m×10^{-3}]	K_1 [kN/m×10^{-3}]	F_y [kN×10^{-3}]	K_2 [kN/m×10^{-3}]	K_1 [kN/m×10^{-3}]	F_y [kN×10^{-3}]
			h/R=0.001					
0.50	47.0	2.3	47.3	203.9	3.1	11.8	168.5	2.5
0.75	81.7	4.1	82.2	354.7	5.3	20.6	293.1	4.4
1.00	123.8	6.2	124.5	537.4	8.1	31.1	444.0	6.7
1.25	169.3	8.5	170.4	735.3	11.0	42.6	607.5	9.1
1.50	216.4	10.8	217.8	939.7	14.1	54.4	776.4	11.6
1.75	264.1	13.2	265.8	1146.8	17.2	66.4	947.5	14.2
2.00	312.0	15.6	314.0	1354.9	20.3	78.5	1119.4	16.8
			h/R=0.004					
0.50	56.3	2.8	56.6	244.4	3.7	14.2	201.9	3.0
0.75	93.2	4.7	93.8	404.8	6.1	23.5	334.5	5.0
1.00	137.5	6.9	138.4	597.2	8.9	34.6	493.4	7.4
1.25	185.3	9.3	186.5	804.7	12.1	46.6	664.9	10.0
1.50	234.6	11.7	236.1	1018.7	15.3	59.0	841.7	12.6
1.75	284.5	14.2	286.3	1235.4	18.5	71.6	1020.7	15.3
2.00	334.6	16.7	336.8	1453.2	21.8	84.2	1200.6	18.0

As part of the isolation systems defined above, supplemental linear viscous dampers providing a total supplemental viscous damping of

$$C = 2 \times \zeta \times M \times \omega_0 \tag{8}$$

are employed, where ζ is the supplemental damping ratio based on the post-yield angular frequency ($\omega_0=2\pi/T_0$) of the isolation system. The effective mass (M) is obtained by dividing the effective weight (W) by the gravitational acceleration. The total supplemental viscous damping coefficients (C) obtained for each base-isolated LST and ζ=10%, 20% and 30% are given in Table 3.

Table 3 - Total supplemental viscous damping coefficients.

H/R	M [kNs^2/m]	C [kNs/m] for h/R=0.001					
		T_0=2 s, ω_0=3.14 rad/s			T_0=4 s, ω_0=1.57 rad/s		
		ζ=10%	ζ=20%	ζ=30%	ζ=10%	ζ=20%	ζ=30%
0.50	4787.8	3008.3	6016.5	9024.8	1504.1	3008.3	4512.4
0.75	8329.2	5233.4	10466.8	15700.2	2616.7	5233.4	7850.1
1.00	12619.4	7929.0	15858.0	23787.1	3964.5	7929.0	11893.5
1.25	17266.0	10848.5	21697.0	32545.6	5424.3	10848.5	16272.8
1.50	22065.2	13864.0	27728.0	41591.9	6932.0	13864.0	20796.0
1.75	26927.1	16918.8	33837.6	50756.4	5459.4	16918.8	25378.2
2.00	31814.3	19989.5	39979.0	59968.6	9994.8	19989.5	29984.3
		C [kNs/m] for h/R=0.004					
0.50	5738.0	3605.3	7210.6	10816.0	1802.7	3605.3	5408.0
0.75	9505.7	5972.6	11945.2	17917.8	2986.3	5972.6	8958.9
1.00	14022.2	8810.4	17620.8	26431.1	4405.2	8810.4	13215.6
1.25	18894.9	11872.0	23744.1	35616.1	5936.0	11872.0	17808.0
1.50	23920.4	15029.6	30059.3	45088.9	7514.8	15029.6	22544.4
1.75	29008.5	18226.6	36453.2	54679.8	9113.3	18226.6	27339.9
2.00	34122.0	21439.5	42878.9	64318.4	10719.7	21439.5	32159.2

2.3. Numerical Modeling

Mathematical models of liquid storage tanks in this study are based on the mechanical model proposed by Haroun and Housner [23], which takes into account the deformation of the tank wall and the sloshing of the liquid inside the tank. This type of modeling concept is illustrated in Figure 4 where the effective masses of m_s, m_f, and m_r are associated with the modes related to the sloshing motion of the fluid, the deformation of the steel wall (fluid-tank interaction) and the non-vibratory part of the liquid that behaves as a rigid body, and moves with respect to the ground above the isolation system, respectively and H_s, H_f and H_r are the effective heights corresponding to the aforementioned masses.

The effective masses, the effective heights and the dominant frequencies of sloshing (ω_s) and fluid-tank (ω_f) modes for tanks filled with water are presented by Haroun and Housner [23]

as a function of H/R and h/R. The readers are referred to Haroun and Housner [23] for the relevant formulations and charts. For the establishment of the mathematical model in this study, the necessary parameters related to the sloshing/convective mode, the fluid-tank mode, and the rigid impulsive mode are given in Tables 4, 5, and 6. In these tables, the sloshing mode period (T_s) and the sloshing mode stiffness (K_s) used in 3D-BASIS-ME modeling are obtained by $T_s=2\times\pi/\omega_s$ and $K_s=\omega_s^2\times m_s$, respectively. Similarly, the fluid-tank mode period (T_f) and the fluid-tank mode stiffness (K_f) values are obtained by $T_f=2\times\pi/\omega_f$ and $K_f=\omega_f^2\times m_f$, respectively. The critical damping ratios of the sloshing and the fluid-tank modes are taken as ζ_s=0.5% [45, 46] and ζ_f=2.0%, respectively. The part of the liquid that moves rigidly and is synchronized with the ground motion without sloshing (i.e. rigid impulsive mode) is modeled to move along with the reinforced concrete basemat. By subtracting the sloshing mode, fluid-tank mode and rigid reinforced concrete basemat weights from the total weight, the weight of the rigidly acting liquid (i.e., rigid impulsive mode weight) is obtained as $W_r = W_t - W_s - W_f - W_{cb}$ and rigid impulsive mode mass is calculated as $m_r = W_r/g$.

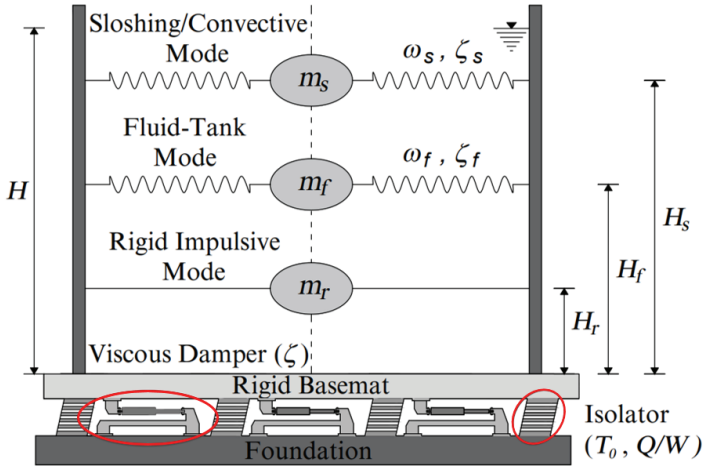

Figure 4 - Mechanical model of base-isolated LSTs.

Table 4 - Characteristic values of the sloshing mode (ζ_s=0.005).

H/R	ω_s [rad/s]	T_s [s]	m_s [kNs^2/m]	K_s [kN/m]	H_s [m]
0.50	0.85	7.42	6379.3	4569.0	4.87
0.75	0.93	6.74	7741.9	6729.3	7.77
1.00	0.97	6.49	8355.7	7838.6	11.07
1.25	0.98	6.39	8613.2	8329.2	14.73
1.50	0.99	6.35	8718.0	8533.1	18.68
1.75	0.99	6.34	8760.1	8615.8	22.83
2.00	0.99	6.33	8776.9	8648.9	27.13

Table 5 - Characteristic values of the fluid-tank mode (ζ_f=0.02).

H/R	*h/R*=0.001				*h/R*=0.004			
	ω_f [rad/s]	T_f [s]	K_f [kN/m×10^{-3}]	H_f [m]	ω_f [rad/s]	T_f [s]	K_f [kN/m×10^{-3}]	H_f [m]
0.50	39.99	0.16	4725.6	3.59	79.98	0.08	20631.8	3.81
0.75	30.30	0.21	5973.2	5.54	60.04	0.10	25276.3	5.78
1.00	24.44	0.26	6427.3	7.68	47.81	0.13	26179.4	7.97
1.25	20.24	0.31	6179.9	10.03	39.54	0.16	24991.8	10.35
1.50	17.05	0.37	5628.4	12.55	33.15	0.19	22416.1	12.91
1.75	14.53	0.43	4939.7	15.22	28.22	0.22	19573.6	15.60
2.00	12.52	0.50	4261.2	18.01	24.23	0.26	16761.6	18.42

3D-BASIS-ME [28] software enables modeling base-isolated LSTs as a mechanical analog with its feature of defining multiple superstructures on a common basemat. Accordingly, single degree of freedom (SDOF) systems representing the fluid sloshing mode, the fluid-tank mode, and the rigid part of the liquid are located on a common basemat supported by an isolation system consisting of isolators and viscous dampers, as schematically shown in Figure 5. The base-isolated LSTs in this study are modeled in 3D-BASIS-ME with this approach and nonlinear seismic response analyses are conducted under historical earthquake records that are described in Section 3. It should be noted here that Scheller and Constantinou [47] showed that there is an excellent agreement between the time history results obtained from 3D-BASIS-ME and SAP2000 programs by making use of the base-isolated LST model presented by Tsopelas et al. [28] which has a similar geometry with the base-isolated tank models used in this study.

Table 6 - Masses.

H/R	m_s [kNs^2/m]	*h/R*=0.001		*h/R*=0.004		m_{cb} [kNs^2/m]
		m_f [kNs^2/m]	m_r [kNs^2/m]	m_f [kNs^2/m]	m_r [kNs^2/m]	
0.50	6379.3	2955.1	639.6	3225.5	1319.5	1192.6
0.75	7741.9	6504.2	632.0	7011.2	1301.5	1192.6
1.00	8355.7	10758.2	668.2	11453.5	1375.6	1192.6
1.25	8613.2	15089.4	983.5	15982.7	1719.1	1192.6
1.50	8718.0	19353.1	1519.0	20396.1	2331.3	1192.6
1.75	8760.1	23389.8	2344.2	24572.9	3242.6	1192.6
2.00	8776.9	27194.8	3426.5	28546.8	4382.1	1192.6

The details of the time integration algorithm used in the nonlinear time history analyses can be found in the 3D-BASIS-ME Technical Report [28]. In summary, the pseudo-force method

originally adopted in 3D-BASIS by Nagarajaiah et al. [40] is used. In this context, while obtaining the solution of the equations of motion and the solution of the differential equations governing the nonlinear behavior of the isolation elements, for each iteration, first, unconditionally stable Newmark's constant-average-acceleration method [48] then an unconditionally stable semi-implicit Runge-Kutta method suitable for stiff differential equations [49] are employed. In order to give an idea on the run time, it should be noted that the analysis for one tank model under TCU101-W ground motion with an Intel Core i7-7700HQ CPU @ 2.80GHz - 2.81 GHz, RAM 16.0 GB Processor is completed in 5.4 s.

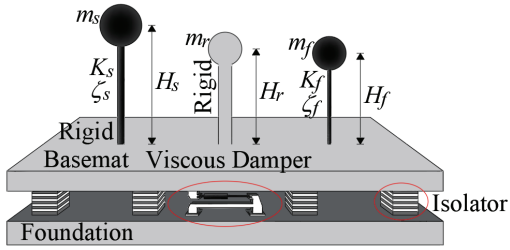

Figure 5 - Schematic representation of base-isolated LST models consisting of SDOF systems sharing a common basemat located on an isolation system equipped with supplemental viscous dampers.

3. EARTHQUAKE DATA

Near-fault earthquakes are pulse-like ground motions observed at locations close to a fault line. They have critical importance in the design of the seismically isolated structures since they may lead to serious seismic demands, particularly in terms of isolator displacements. These earthquake records differ from far-fault ones recorded further away from the seismic source by distinct pulses with high-amplitude and long-periods observed in the velocity time histories [17-19]. Although the aforementioned characteristic features of near-fault earthquakes were first revealed by Housner and Trifunac [15] while examining the records of the 1966 Parkfield earthquake at Cholame [50, 51], it was first addressed by Bertero et al. [52] that the flexible structures are vulnerable to severe effects of near-fault earthquakes. They associated the damage of the buildings of the Olive View Medical Center during the 1971 San Fernando California earthquake with near-fault earthquake effects [53]. However, this potential problem has attracted most engineers' attention, only after the 1994 Northridge, California Earthquake that occurred in a heavily urbanized area [54]. In this context, Hall et al. [55] and Heaton et al. [56] emphasized that the necessity of developing appropriate design codes to prevent the potential destructive effects of near-fault earthquakes by examining the seismic performance of flexible high-rise and seismically isolated buildings under the effect of a simulated M_w 7.00 earthquake on a blind thrust fault.

Until today, various studies have been carried out examining seismically isolated structures from different perspectives under near-fault earthquakes. Among these, base-isolated LSTs are of particular importance because both the period of the isolation system and the sloshing mode period of such structures may coincide with the velocity pulse periods of the near-fault earthquakes, resulting in very large isolation system and sloshing displacements. As

explained in Introduction section, supplemental viscous dampers may be employed at the base-isolation systems of LSTs in order to prevent large base displacements (i.e. isolation system displacements) that may occur under near-fault earthquakes but this may cause increases in the seismic demands of the superstructure in case of far-fault earthquakes. In order to examine both situations, in this study, twelve historical earthquake records, six representing near-fault and six representing far-fault earthquakes, are obtained from University of California, Berkeley PEER Ground Motion Database [57] for use in the nonlinear time history analyses. Information on these records is presented in Table 7 where M_w, r, PGA, PGV, T_p, VSI, and HI represent the moment magnitude, the fault-distance, the peak ground acceleration, the peak ground velocity, the predominant period (for far-fault earthquakes)/the pulse period (for near-fault earthquakes), the Velocity Spectrum Intensity, and the Housner Intensity, respectively. As it can be seen from Table 7, for the near-fault earthquake records, the closest distances to the fault lines are less than 10 km and PGV values vary from 40.6 cm/s to 166.1 cm/s. On the other hand, for the far-fault records, the fault-distances are more than 10 km (from 10.30 to 19.30 km) and PGV values are much less than those of near-fault ones and vary from 19.7 to 44.6 cm/s.

Table 7 - Characteristics of historical near-fault and far-fault earthquake records.

Near-fault									
Earthquake	M_w	Component	Station Name	r [km]	PGA [g]	PGV [cm/s]	T_p [s]	VSI [cm]	HI [cm]
Chi-Chi	7.6	TCU052-W	TCU052	0.24	0.348	159.0	2.48	318.3	382.5
Erzincan	6.9	ERZ-NS	Erzincan	2.00	0.515	83.9	2.40	297.0	319.9
Chi-Chi	7.6	TCU101-W	TCU101	2.94	0.202	67.9	3.98	114.7	119.2
Loma Prieta	6.9	LGP000	LGPC	6.10	0.563	94.8	3.22	431.4	409.8
Northridge	6.7	RRS228	Rinaldi Receiving Sta.	7.10	0.838	166.1	1.42	509.7	456.8
Northridge	6.7	ARL090	Arleta-Nordhoff Fire Sta.	9.20	0.344	40.6	1.06	146.2	130.1
Far-fault									
Loma Prieta	6.9	BRN-090	BRAN	10.30	0.501	44.6	0.14	165.1	120.8
Northridge	6.7	RO3-090	Sun Valley-Roscoe Blvd.	12.30	0.443	38.2	0.16	173.7	165.7
Loma Prieta	6.9	CAP000	Capitola	14.50	0.529	36.5	0.28	207.4	187.0
Chi-Chi	7.6	CHY029-W	CHY029	15.28	0.277	30.3	0.46	125.4	116.7
Loma Prieta	6.9	WAH-090	WAHO	16.90	0.638	38.0	0.14	147.9	127.9
Northridge	6.7	SSU-090	Santa Susana Ground	19.30	0.290	19.7	0.33	89.2	78.2

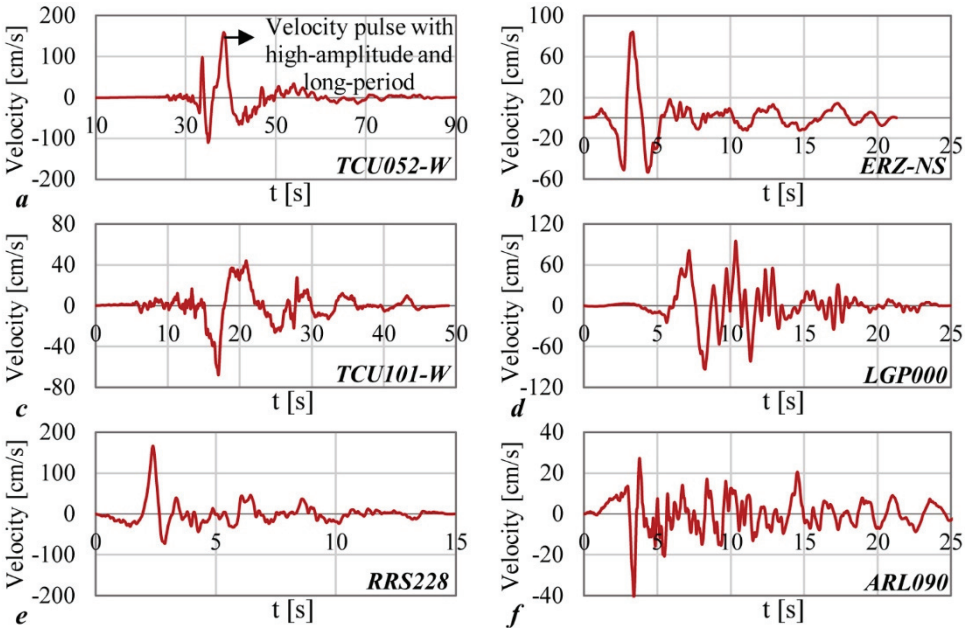

Figure 6 - Velocity time histories of near-fault earthquake records - (a) TCU052-W, (b) ERZ-NS, (c) TCU101-W, (d) LGP000, (e) RRS228, and (f) ARL090.

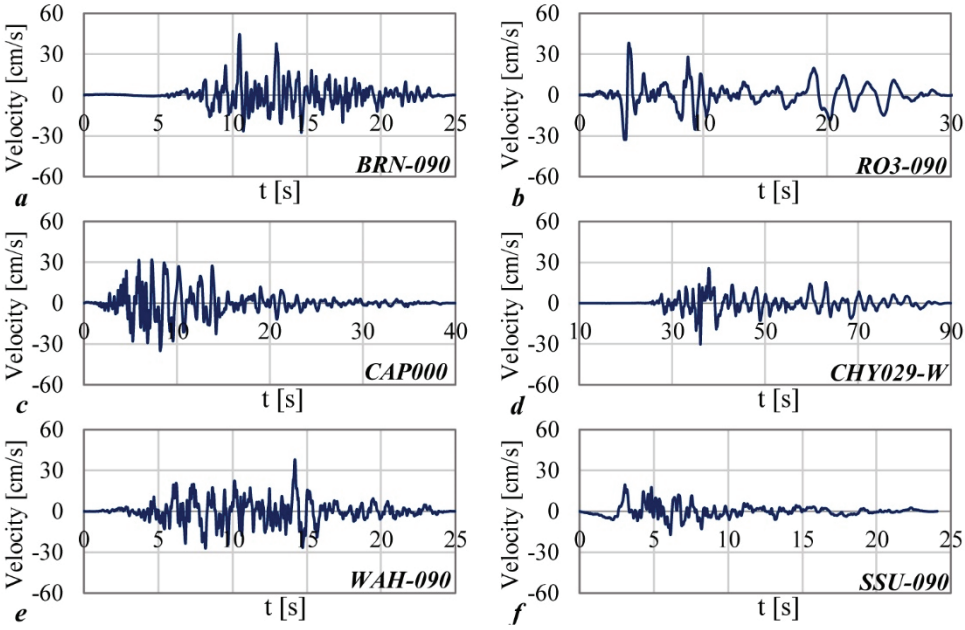

Figure 7 - Velocity time histories of far-fault earthquake records - (a) BRN-090, (b) RO3-090, (c) CAP000, (d) CHY029-W, (e) WAH-090, and (f) SSU-090.

Figures 6 and 7 present the velocity time histories of near-fault and far-fault earthquake records, respectively. Similar to what was pointed out in the previous studies [18, 26, 58], it is seen from Figure 6 that the near-fault earthquake records contain large-amplitude and long-period velocity pulses ranging from 1.06 s to 3.98 s as presented in Table 7, which would amplify the responses of base-isolated LSTs. On the other hand, far-fault earthquake records do not contain any velocity pulses (Figure 7). Also, the Housner Intensity and Velocity Spectrum Intensities for the near-fault earthquake records are much larger (ranging from 130.1 cm to 509.7 cm) compared to those for far-fault earthquake records (ranging from 78.2 cm to 207.4 cm). This also is an indicator of the much larger seismic demands near-fault earthquake records would have on the base-isolated LSTs considered in this study.

4. DISCUSSION OF RESULTS

Base-isolated LSTs obtained by combining different parameters including the properties of the tank geometry (H/R and h/R) and the properties of the base-isolation system (T_0 and ζ) as described in detail in Section 2 are modeled numerically in 3D-BASIS-ME and subjected to six near-fault (TCU052-W, ERZ-NS, TCU101-W, LGP000, RRS228, and ARL090) and six far-fault (BRN-090, RO3-090, CAP000, CHY029-W, WAH-090, and SSU-090) historical earthquake records whose characteristic features are described in detail in Section 3. As a result of the nonlinear time history analyses, structural responses including the base displacement, the sloshing displacement, and the isolation system shear force are obtained and reported here. Normalized isolation system shear forces are obtained by proportioning the isolation system shear forces to the total weight of the superstructure on the isolation system.

4.1. Response Time Histories

Although the assessments here are made using the peak values, in order to also portray the time history behavior visually, first, the time variation of aforementioned structural responses are presented in Figure 8 for a sample base-isolated LST model with T_0=4 s, ζ=20%, H/R=1.25 and for TCU052-W and CAP000, only, as representatives of near-fault and far-fault earthquakes, respectively. This figure shows that the TCU052-W near-fault earthquake leads to significantly higher responses in comparison with the CAP000 far-fault earthquake. It is also observed that while the far-fault earthquake responses in terms of base displacement and isolation system shear force contain high-frequency parts, counterpart near-fault responses show pulse-like nature. Differently, the sloshing displacement responses both in case of far-fault and near-fault earthquakes have long-periods and the sloshing continues even after the earthquake comes to an end due to the very low sloshing mode damping.

4.2. Peak Responses

The complete picture of the study in terms of peak responses are presented in Figures 9-11. The peak base displacement, the peak sloshing displacement, and the normalized peak isolation system shear force demands for all considered cases and parameters are shown in Figures 9, 10, and 11, respectively. It should be noted here that these and other remaining

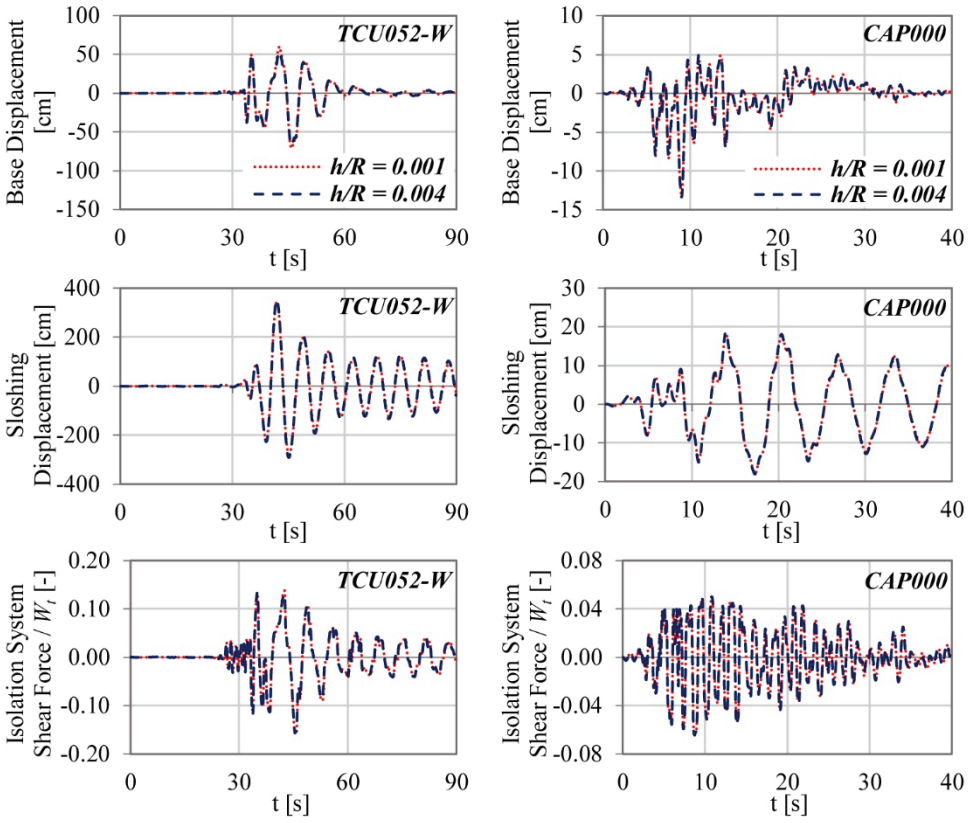

Figure 8 - Time histories of the structural responses for base-isolated LSTs with T_0=4 s, ζ=20%, H/R=1.25 under near-fault TCU052-W and far-fault CAP000 earthquakes.

figures in this paper are presented for h/R=0.001, only, since the influence of this parameter which is related to tank thickness/flexibility are rather limited as demonstrated in Figure 8 that compares the time histories of the structural responses for h/R=0.001 and h/R=0.004. A more detailed discussion regarding this issue is presented in Section 4.3.1.

As seen in Figures 9-11, the structural responses vary in a wide range depending on the characteristic of the earthquake record (i.e. moment magnitude (M_w), the fault-distance (r), near-fault vs. far-fault), the slenderness of the tank (i.e. H/R ratio), the isolation period (T_0), and the level of viscous supplemental damping (ζ).

As a common observation, the structural responses obtained in case of near-fault earthquakes are significantly higher than those obtained for far-fault earthquakes. While the peak base displacement can be as high as 132.54 cm in case of near-fault earthquakes (for TCU052-W, H/R=0.50, T_0=4 s), the highest value is only 17.10 cm in case of far-fault earthquakes (for CAP000 earthquake and T_0=2 s). Therefore, it is seen that supplemental damping may be required when LSTs with long-period isolation systems are subjected to large magnitude near-fault earthquakes.

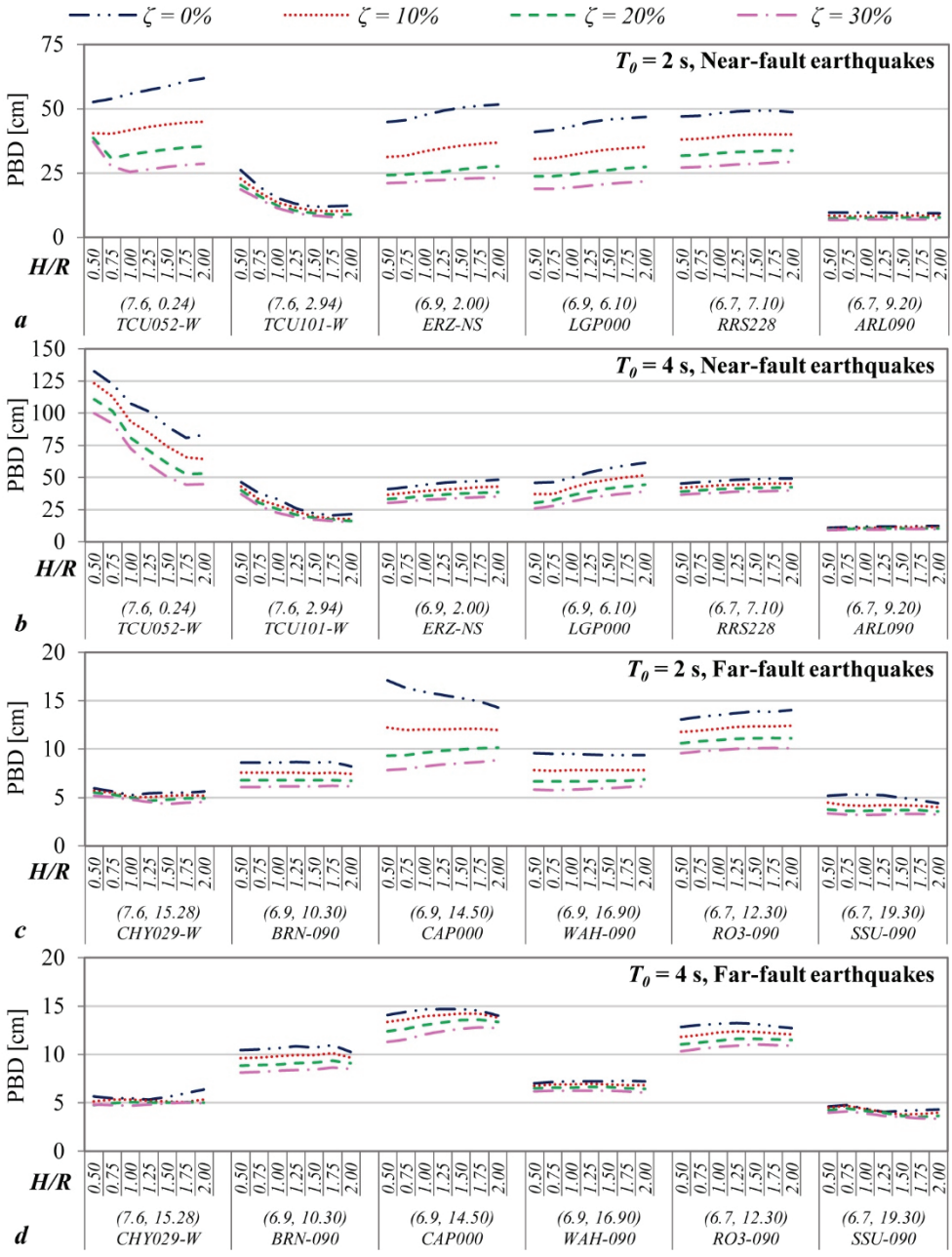

Figure 9 - Peak base displacement (PBD) demands for near-fault and far-fault earthquakes. (Values in parenthesis are the moment magnitude, M_w, and the fault-distance, r).

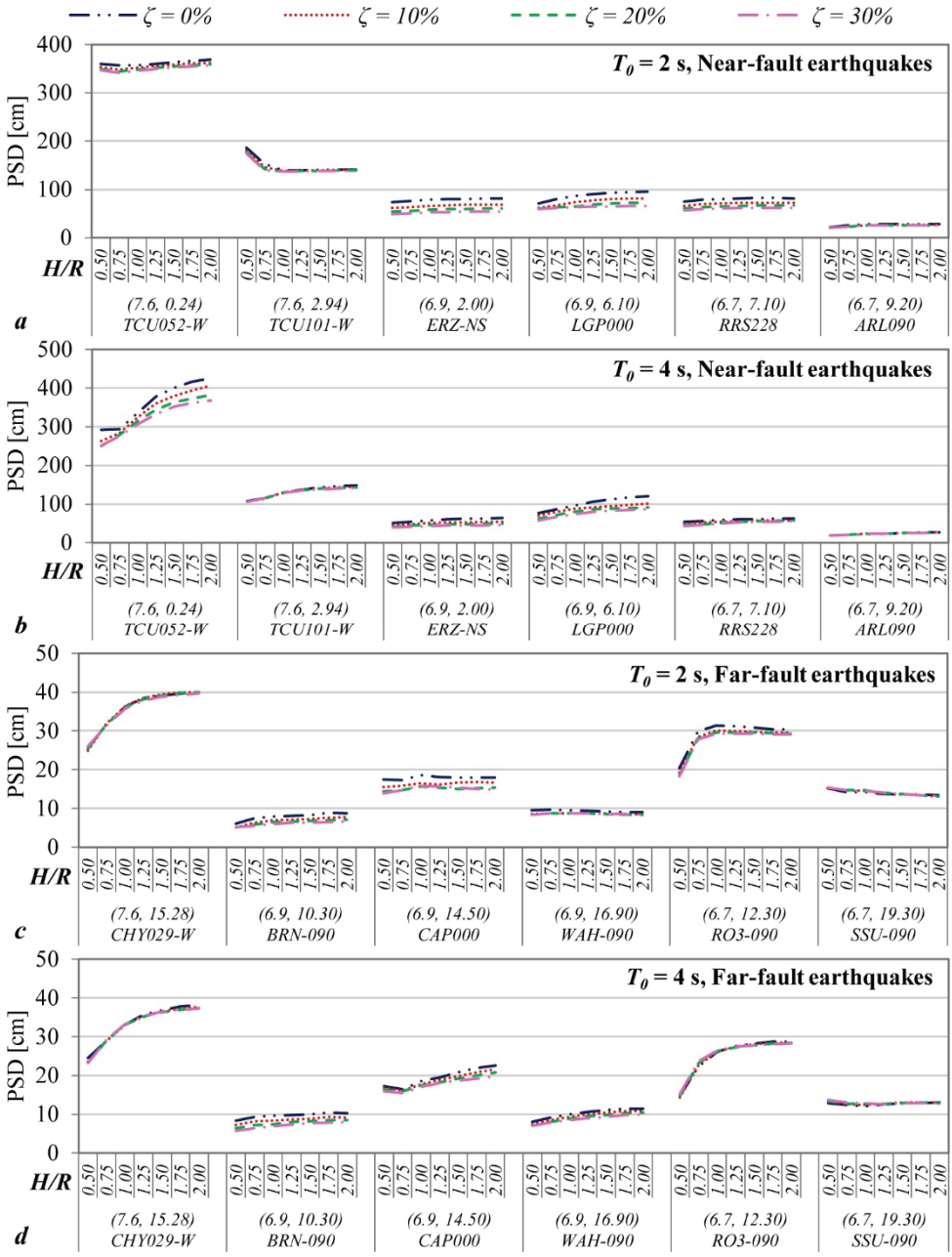

Figure 10 - Peak sloshing displacement (PSD) demands for near-fault and far-fault earthquakes. (Values in parenthesis are the moment magnitude, M_w, and the fault-distance, r).

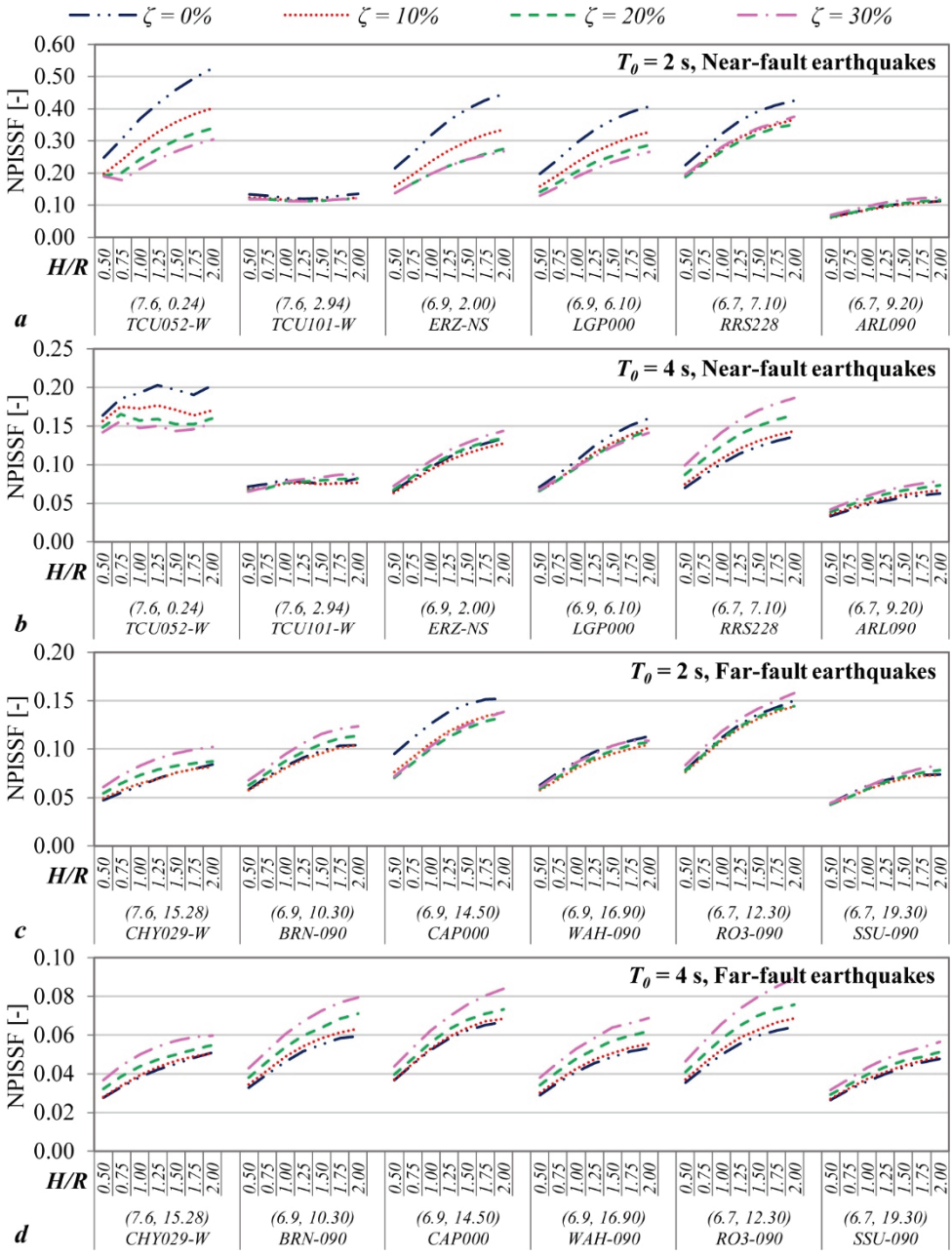

Figure 11 - Normalized peak isolation system shear force (NPISSF) demands for near-fault and far-fault earthquakes. (Values in parenthesis are the moment magnitude, M_w, and the fault-distance, r).

Likewise, the sloshing displacement demands may be extremely high in near-fault earthquakes, with the largest being 425.20 cm observed for TCU052-W, H/R=2.00, and T_0=4 s. On the other hand, the largest peak sloshing displacement demand in case of far-fault earthquakes was only 40.0 cm which is obtained for CHY029-W. The peak isolation system shear force values also yield a similar trend. While the largest demand in terms of this structural response is 0.16 in case of far-fault earthquakes (for RO3-090, H/R=2.00, T_0=2 s), it is about 3.3 times larger, i.e. 0.53, in case of near-fault earthquakes (for TCU052-W, H/R=2.00, T_0=2 s).

Another observation is that while the demands quickly decrease as the fault-distance increases in case of near-fault earthquakes, such a clear trend is not observed in case of far-fault earthquakes. In particular, TCU052-W, which is recorded at only 0.24 km away from the fault line, dissociates from other earthquake records which results in very high demands especially for long-period isolation systems and in terms of base displacement and sloshing displacement. The supplemental viscous damping proved to be very successful in this case by reducing the peak base displacement demands from 83.03 ~ 132.54 cm range realized for ζ=0% to 44.17 ~ 99.90 cm range realized for ζ=30% (depending on H/R). Furthermore, even the peak sloshing displacement demands, which may be classified as part of the superstructure response, are suppressed from 292.35 ~ 425.20 cm realized for ζ=0% to 251.94 ~ 367.79 cm range realized for ζ=30%.

4.3. Average Peak Responses and General Trends

In order to bring out the general trends as a function of the parameters examined herein, the average values of the peak base displacement, the peak sloshing displacement, and the normalized isolation system shear force demands are presented in Figures 12, 13, and 14, respectively, in a comparative fashion both for near-fault and far-fault earthquakes. The influences of the tank flexibility, h/R, the tank slenderness ratio, H/R, the isolation system period, T_0, and the supplemental viscous damping ratio, ζ, on the behavior of base-isolated LSTs equipped with supplemental viscous dampers under near-fault and far-fault earthquakes are discussed by making use of these plots in Sections 4.3.1-4.3.4.

4.3.1. Influence of the Tank Flexibility, h/R

Figure 8 compares the time histories of the structural responses for tank flexibility ratios of h/R=0.001 and h/R=0.004 for the sample base-isolated LST model with T_0=4 s, ζ=20%, H/R=1.25 under TCU052-W and CAP000 which are meant to represent near-fault and far-fault earthquakes, respectively. It is observed that the influence of tank flexibility, i.e. the influence of tank-fluid interaction, on both the superstructure and the isolation system responses are much less than the other parameters (i.e., H/R, T_0, and ζ) and negligibly small. This finding is in line with other studies on base-isolated LSTs without supplemental dampers [e.g., 59-61]. Besides, Safari and Tarinejad [27] reported that the effect of the tank flexibility on the sloshing displacement, the isolator displacement, and the base shear demands generally can be neglected.

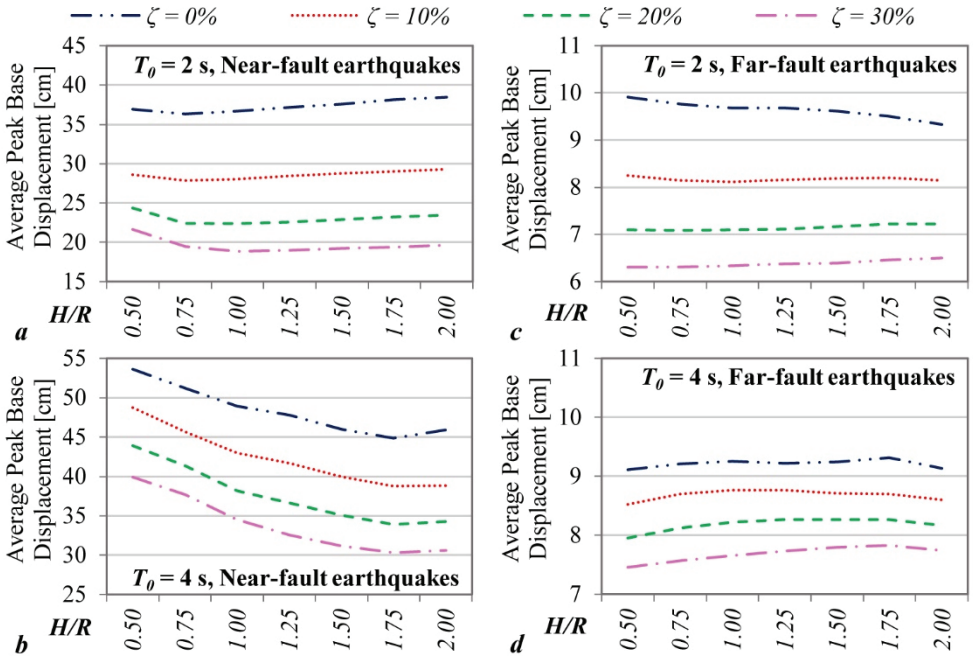

Figure 12 - Average peak base displacement demands.

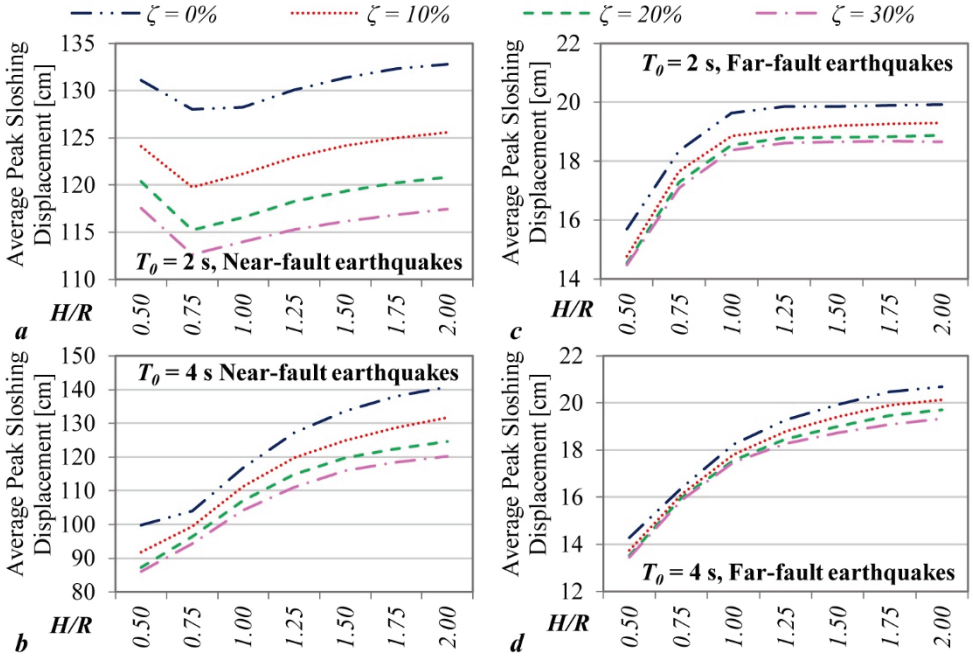

Figure 13 - Average peak sloshing displacement demands.

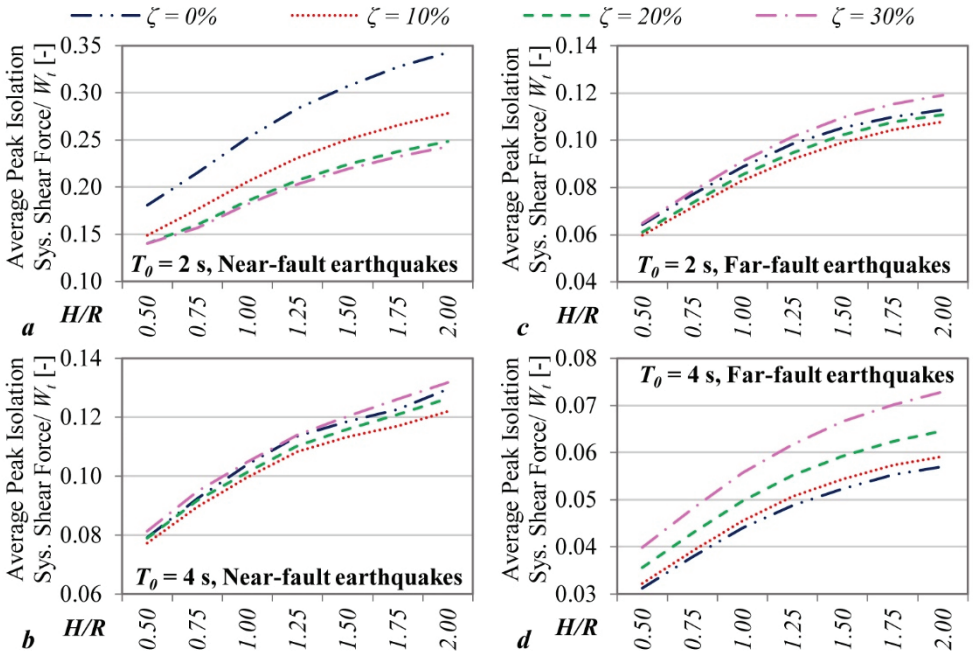

Figure 14 - Average normalized peak isolation system shear force demands.

4.3.2. Influence of the Tank Slenderness Ratio, H/R

It is observed that the increase in the tank slenderness ratio, *H/R*, could increase or decrease the peak base displacement demands depending on the characteristics of the earthquake (see Figure 12). Although there is no clear trend, it is important to observe that the tank slenderness ratio may have considerable effects on the peak base displacement demands particularly in case of LSTs with long-period isolation systems. As it can be seen from Figure 12, in case of long-period T_0=4 s isolation systems under near-fault earthquakes, the change in the average peak base displacement demands is about 20% as *H/R* varies from 0.50 to 2.00.

When Figure 13 is examined, the increase in the tank slenderness ratio, *H/R*, generally increases the peak sloshing displacement demands for both near-fault and far-fault earthquakes. While the extent of this increase varies depending on the characteristics of the individual earthquake record, the effect is more significant in case of long-period T_0=4 s isolation systems and the change in the average peak sloshing displacement demands is about 40% as *H/R* varies from 0.50 to 2.00.

Normalized peak isolation system shear forces increase both under the near-fault and the far-fault earthquakes with the increase in the tank slenderness ratio, *H/R*. As seen in Figure 14, the increase observed in the average normalized peak isolation system shear force responses is significant and varies in the range of about 60 to 90% as *H/R* varies from 0.50 to 2.00.

4.3.3. Influence of the Isolation System Period, T_0

As shown in Figure 12, the peak base displacement demands for the short-period base-isolated LSTs with T_0=2 s are smaller than long-period ones with T_0=4 s for both near-fault and far-fault earthquakes. This is much more pronounced in case of near-fault earthquakes where the peak base displacement demands of long-period isolation systems may be higher than that of the short-period isolation system as much as 84.48% as observed for H/R=0.50, ζ=30% case. Under the far-fault earthquakes, although the increase in the isolation system period results in a higher peak base displacement demand, it is not as dramatic as is the case for near-fault earthquakes. The largest increase in this case is about 22%. Furthermore, although exceptional, there may be cases for which the increase in the isolation period results in a decrease in the peak base displacement under far-fault earthquakes. For example, for H/R=0.50, ζ=0%, this decrease is 8.07%.

It is seen from Figure 13 that increasing the isolation period decreases the peak sloshing displacement demand under near-fault and far-fault earthquakes for squat tanks with H/R values smaller than 1.00. This effect is most pronounced for the smallest H/R and in case of near-fault earthquakes where the reduction in the peak sloshing displacement demand may increase to 27.54%. However, for slender tanks with H/R values greater than 1.00, this trend is reversed and short-period isolation systems result in slightly smaller peak sloshing displacement demands. In case of the highest H/R value of 2.00, this reduction is on the order of 5%.

It is observed that the normalized peak isolation system shear force responses of the tanks with long-period isolation systems (T_0=4 s) are about 50% smaller than the tanks with short-period isolation systems (T_0=2 s) under both near-fault and far-fault earthquake records (Figure 14). This trend is valid for all cases examined without any exception.

4.3.4. Influence of the Supplemental Viscous Damping Ratio, ζ

Figures 12-14 demonstrate the significant influence of the use of supplemental viscous dampers on the seismic behavior of base-isolated LSTs. As discussed in detail in Sections 4.1 and 4.2, the need for supplemental viscous damping is especially seen when the structure is subjected to near-fault earthquakes and this need rises even more as the fault-distance decreases. However, it should be kept in mind that typically a structure is threatened by more than one fault at various distances and thus potentially hit by both near-fault and far-fault earthquakes during its lifetime. The supplemental dampers provided against near-fault earthquakes will be there and thus act when the same structure is hit by a far-fault earthquake. Therefore, it is essential to assess the seismic behavior not only under near-fault earthquakes but also under far-fault earthquakes since negative effects of high damping may come into scene in the superstructure responses.

As it can be seen in Figure 12, supplemental viscous dampers reduce the peak base displacement demands with respect to no supplemental viscous damper case and increasing damping ratios from 10 to 30% steadily decrease the displacement demands. The reduction obtained for ζ=30% varies in the range of 25 ~ 50% among the examined cases. This behavior is valid for all base-isolated LSTs examined herein and for both near-fault and far-fault earthquakes.

Figure 13 shows the effect of supplemental viscous damping on the peak sloshing displacement demands. As seen, although use of supplemental viscous dampers reduce this demand for both near-fault and far-fault earthquakes, the extent of the reduction is modest, i.e. varies 10~15 among the examined cases even for ζ=30% as compared to no damper (ζ=0%) case. The effectiveness of the supplemental viscous dampers in terms of reducing peak sloshing displacement demands are more for slender tanks and less for squat tanks. It should be noted here that there may be exceptions on an individual record basis where the use of supplemental viscous dampers at the base-isolation system causes amplification in the peak sloshing displacement, which is a superstructure response (Figure 10). For example, under the SSU-090 earthquake record, adding supplemental damping with ζ=30% increases the peak sloshing displacement demand by 7.67% with respect to no supplemental damper case for H/R=1.00 and T_0=4 s.

The supplemental viscous dampers have complex effects on the peak isolation system shear force demands. In case of near-fault earthquakes -except for very high damping (ζ=30%) in case of long-period (T_0=4 s) isolation systems- increasing supplemental viscous damping ratio decreases this demand. However, for far-fault earthquakes, it is clearly seen that increasing supplemental viscous damping ratio increases the peak isolation system shear force demand, which is a superstructure response parameter.

5. CONCLUSIONS

Employing seismic isolation at the base of liquid storage tanks (LSTs) is an effective way of protecting these critical structures from the detrimental effects of earthquakes. For those located in the near-fault regions, use of supplemental viscous dampers may be essential for reducing the base displacements to acceptable values, which may on the other hand cause increase in the superstructure demands in case of far-fault earthquakes. The success of such hybrid base-isolation systems depends on the characteristics of the earthquake, the isolation system properties, and the superstructure properties. In this study, in order to determine the influence of the supplemental viscous damping ratio (ζ), the isolation system period (T_0), the tank wall flexibility, i.e. the ratio of the steel tank wall thickness to the tank radius (h/R), and the slenderness ratio, i.e. the ratio of the water height to the tank radius (H/R) on the seismic responses including the base displacement, the sloshing displacement, and the isolation system shear force demands normalized by total superstructure weight, a parametric investigation is carried out via nonlinear seismic response analyses of benchmark base-isolated LSTs with supplemental viscous dampers under six near-fault and six far-fault historical earthquake records.

Based on the results of the analyses conducted, following conclusions are reached:

- As a common observation, structural responses generally increase exponentially as the fault-distance decreases. Under some earthquake records, this increase may be much more pronounced for the base and sloshing displacement demands especially for long-period isolation systems which may be considerably increased or decreased depending on the tank slenderness ratio.
- While supplemental viscous damping is very successful in reducing high base displacement demands in near-fault cases to acceptable levels, the extent of the reduction

is modest in terms of sloshing displacement demands. There may even be exceptions where supplemental viscous dampers cause slight amplifications on the sloshing displacement, which is a superstructure response. And, the effectiveness of the supplemental viscous dampers in terms of reducing sloshing displacement demands are more for slender tanks with *H/R* values larger than 1.00 and less for squat tanks with *H/R* values smaller than 1.00.

- In case of near-fault earthquakes -except for high damping (ζ=30%)- increasing supplemental viscous damping decreases the isolation system shear force. However, employing and increasing supplemental viscous damping increase the isolation system shear force -a superstructure response- in case of far-fault earthquakes.
- Under both near-fault and far-fault earthquakes, while increasing the isolation period decreases the sloshing displacement demand for squat tanks, it slightly reduces the sloshing displacement demand for slender tanks. Especially for long-period isolation systems, increase in the tank slenderness ratio generally increases the sloshing displacement demands.
- Normalized isolation system shear force demands are greater for short-period isolation systems and increase with the increase in the tank slenderness ratio under both near-fault and far-fault earthquakes.
- The influence of tank flexibility, i.e. tank-fluid interaction, on both the superstructure and the isolation system responses is negligibly small for LSTs with hybrid base-isolation systems. This finding is in line with other studies in the literature on base-isolated LSTs without supplemental dampers.

The conclusions above are drawn by neglecting the wave-wave, wave-wall and wave-roof interactions. These interactions may be important especially in case of high amplitude vibrations. Therefore, further investigations considering these interactions particularly in case of near-fault earthquakes should be carried out as part of the future studies.

Acknowledgment

A part of this work was supported by the Scientific and Technological Research Council of Turkey (TÜBİTAK). Project Number: 214M633.

References

[1] Lee, S., Kim, B., Lee, Y-J., Seismic Fragility Analysis of Steel Liquid Storage Tanks using Earthquake Ground Motions Recorded in Korea. Math. Probl. Eng., Article ID 6190159, 15 pages, 2019.

[2] Zhao, Z., Lu, X., Guo, Y., Zhao, X., Seismic Fragility Assessment of Base-Isolated Steel Water Storage Tank. Shock Vib., Article ID 8835943, 13 pages, 2020.

[3] Tsipianitis, A., Tsompanakis, Y., Optimizing the Seismic Response of Base-Isolated Liquid Storage Tanks using Swarm Intelligence Algorithms. Comput. Struct., 243, 106407, 2021.

[4] Hatayama, K., Lessons from the 2003 Tokachi-oki, Japan, Earthquake for Prediction of Long-Period Strong Ground Motions and Sloshing Damage to Oil Storage Tanks. J. Seismol., 12, 255-263, 2008.

[5] Yazici, G., Cili, F., Evaluation of the Liquid Storage Tank Failures in the 1999 Kocaeli Earthquake. 14th World Conference on Earthquake Engineering, Beijing, China, 2008.

[6] Jadhav, M.B., Jangid, R.S., Response of Base-Isolated Liquid Storage Tanks. Shock and Vibration, 11, 33-45, 2004.

[7] Shrimali, M.K., Jangid, R.S., Seismic Analysis of Base-Isolated Liquid Storage Tanks. Journal of Sound and Vibration, 275(1), 59-75, 2004.

[8] Jadhav, M.B., Jangid, R.S., Response of Base-Isolated Liquid Storage Tanks to Near-Fault Motions. Structural Engineering and Mechanics, 23(6), 615-634, 2006.

[9] Shekari, M.R., Khaji, N., Ahmadi, M.T., On the Seismic Behavior of Cylindrical Base-Isolated Liquid Storage Tanks Excited by Long-Period Ground Motions. Soil Dynamics and Earthquake Engineering, 30, 968-980, 2010.

[10] Panchal, V.R., Soni, D.P., Seismic Behaviour of Isolated Fluid Storage Tanks: A-State-of-the-Art Review. KSCE J. Civ. Eng., 18(4), 1097-1104, 2014.

[11] Saha, S.K., Matsagar, V., Chakraborty, S., Uncertainty Quantification and Seismic Fragility of Base-Isolated Liquid Storage Tanks using Response Surface Models. Probabilistic Eng. Mech., 43, 20-35, 2016.

[12] Hashemi, S., Aghashiri, M.H., Seismic Responses of Base-Isolated Flexible Rectangular Fluid Containers under Horizontal Ground Motions. Soil Dyn. Earthq. Eng., 100, 159-168, 2017.

[13] Alhan, C., Gazi, H., Güler, E., Influence of Isolation System Characteristic Strength on the Earthquake Behavior of Base-Isolated Liquid Storage Tanks. Indian J. Eng. Mater. Sci., 25(4), 346-352, 2018.

[14] Tsipianitis, A., Tsompanakis, Y., Impact of Damping Modeling on the Seismic Response of Base-Isolated Liquid Storage Tanks. Soil Dynamics and Earthquake Engineering, 121, 281-292, 2019.

[15] Housner, G.W., Trifunac, M.D., Analysis of Accelerograms-Parkfield Earthquake. Bull. Seismol. Soc. Am., 57(6), 1193-220, 1967.

[16] Makris, N., Rigidity-Plasticity-Viscosity: Can Electrorheological Dampers Protect Base Isolated Structures from Near-Source Ground Motions? Earthq. Eng. Struct. Dyn., 26, 571-591, 1997.

[17] Bray, J.D., Rodriguez-Marek, A., Characterization of Forward-Directivity Ground Motions in the Near-Fault Region. Soil Dyn. Earthq. Eng., 24, 815-828, 2004.

[18] He, W.L., Agrawal, A.K., An Analytical Model of Ground Motion Pulses for the Design and Assessment of Smart Protective Systems. ASCE J. Struct. Eng., 134(7), 1177-1188, 2008.

[19] Kanbir, Z., Alhan, C., Özdemir, G., Influence of Superstructure Modeling Approach on the Response Prediction of Buildings with LRBs Considering Heating Effects. Structures, 28, 1756-1773, 2020.

[20] Hall, J.F., Seismic Response of Steel Frame Buildings to Near-Source Ground Motions. Earthq. Eng. Struct. Dyn., 27, 1445-1464, 1998.

[21] Somerville, P.G., Graves, R.W., Characterization of Earthquake Strong Ground Motion. Pure Appl. Geophys., 160, 1811-1828, 2003.

[22] Alhan, C., Güler, E., Gazi, H., Behavior of Base-Isolated Liquid Storage Tanks under Synthetic Near-Fault Earthquake Pulses. 5th International Symposium on Life-Cycle Civil Engineering, Delft, Holland, 515, 2415-2419, 2016.

[23] Haroun, M.A., Housner, G.W., Seismic Design of Liquid Storage Tanks. Journal of the Technical Councils of ASCE, 107, 191-207, 1981.

[24] Kalogerakou, M.E., Maniatakis, C.A., Spyrakos, C.C., Psaropoulos, P.N., Seismic Response of Liquid-Containing Tanks with Emphasis on the Hydrodynamic Response and Near-Fault Phenomena. Eng. Struct., 153, 383-403, 2017.

[25] Housner, G.W., Earthquake Pressures on Fluid Containers, Tech. Rep. NR-081-095, California Institute of Technology, Pasadena, California, 1954.

[26] Öncü-Davas, S., Gazi, H., Güler, E., Alhan, C., Comparison of Ground Motion Pulse Models for the Seismic Response of Seismically Isolated Liquid Storage Tanks, Earthquake Engineering and Structural Dynamics in Memory of Ragnar Sigbjörnsson, In: Rupakhety, R. and Ólafsson, S., (eds.), Chapter 7, Springer International Publishing AG, Geotechnical, Geological and Earthquake Engineering, 143-157, 2018.

[27] Safari, S., Tarinejad, R., Parametric Study of Stochastic Seismic Responses of Base-Isolated Liquid Storage Tanks under Near-Fault and Far-Fault Ground Motions. J. Vib. Control, 24, 5747-5764, 2018.

[28] Tsopelas, P.C., Constantinou, M.C., Reinhorn, A.M., 3D-BASIS-ME: Computer Program for Nonlinear Dynamic Analysis of Seismically Isolated Single and Multiple Structures and Liquid Storage Tanks, Tech. Rep. NCEER-94-0010, National center for earthquake engineering research, State Univ. of New York, Buffalo, NY, 1994.

[29] Castellano, M.G., Infanti, S., Dumoulin, C., Ducoup, L., Martelli, A., Dusi, A., Shaking Table Tests on a Liquefied Natural Gas Storage Tank Mock-up Seismically Protected with Elastomeric Isolators and Steel Hysteretic Torsional Dampers. 12th World Conference on Earthquake Engineering, Auckland, New Zealand, 2000.

[30] Gazi, H., Kazezyılmaz-Alhan, C.M., Alhan, C., Behavior of Seismically Isolated Liquid Storage Tanks Equipped with Nonlinear Viscous Dampers in Seismic Environment. 10th Pacific Conference on Earthquake Engineering, Sydney, Australia, 2015.

[31] Luo, H., Zhang, R., Weng, D., Mitigation of Liquid Sloshing in Storage Tanks by using a Hybrid Control Method. Soil Dyn. Earthq. Eng., 90, 183-195, 2016.

[32] Güler, E., Alhan, C., Performance Limits of Base-Isolated Liquid Storage Tanks with/without Supplemental Dampers under Near-Fault Earthquakes. Structures, 33, 355-367, 2021.

[33] Tsipianitis, A., Tsompanakis, Y., Improving the Seismic Performance of Base-Isolated Liquid Storage Tanks with Supplemental Linear Viscous Dampers. Earthq. Eng. Eng. Vib., 21, 269-282, 2022.

[34] Bakalis, K., Fragiadakis, M., Vamvatsikos, D., Surrogate Modeling for the Seismic Performance Assessment of Liquid Storage Tanks. Journal of Structural Engineering, 143(4): 1–13, 2017.

[35] Güler, E., Effect of Supplemental Damping on the Earthquake Behavior of Base-Isolated Liquid Storage Tanks, Ph.D. Thesis, Istanbul University-Cerrahpaşa, Institute of graduate studies, 2019.

[36] Malhotra, P.K., Wenk, T., Wieland, M., Simple Procedure for Seismic Analysis of Liquid-Storage Tanks. Struct. Eng. Int., 3, 197-201, 2000.

[37] Shrimali, M.K., Jangid, R.S., Seismic Analysis of Base-Isolated Liquid Storage Tanks. J. Sound Vib., 275, 59-75, 2004.

[38] Seleemah, A.A., El-Sharkawy, M., Seismic Response of Base Isolated Liquid Storage Ground Tanks. Ain Shams Eng. J., 2(1), 33-42, 2011.

[39] Compagnoni, M.E., Curadelli, O., Ambrosini, D., Experimental Study on the Seismic Response of Liquid Storage Tanks with Sliding Concave Bearings. J. Loss Prev. Process Ind., 55, 1-9, 2018.

[40] Nagarajaiah, S., Reinhorn, A.M., Constantinou, M.C., 3D-BASIS: Nonlinear Dynamic Analysis of Three-Dimensional Base Isolated Structures, Tech. Rep. NCEER-89-0019, National Center for Earthquake Engineering Research, State University of New York, Buffalo, NY, 1989.

[41] Bouc, R., Forced Vibrations of a Mechanical System with Hysteresis. 4th Conference on Non-linear Oscillations, Prague, Czechoslovakia, pp. 315, 1967.

[42] Wen, Y.K., Method for Random Vibration of Hysteretic Systems. J. Eng. Mech. Div., 102, 246-263, 1976.

[43] Park, Y., Wen, Y., Ang, A., Random Vibration of Hysteretic Systems under Bi-directional Ground Motions. Earthquake Eng. Struct. Dyn., 14, 543–557, 1986.

[44] Naeim, F., Kelly, J.M., Design of Seismic Isolated Structures: From Theory to Practice, 978-0-471-14921-7, John Wiley & Sons, New York, 1999.

[45] Eurocode 8: EN1998. Design of Structures for Earthquake Resistance, Part 4: Silos, Tanks and Pipelines, Brussels, Belgium, 2006.

[46] ASCE 7. Minimum Design Loads and Associated Criteria for Buildings and Other Structures, ASCE/SEI 7-16, Reston, Virginia, 2017.

[47] Scheller, J., Constantinou, M.C., Response History Analyses of Structures with Seismic Isolation and Energy Dissipation Systems: Verification Examples for Program SAP2000, Technical Report MCEER-99-0002, University at Buffalo, New York, 1999.

[48] Newmark, N.M., A Method of Computation for Structural Dynamics, J. of Engrg. Mech. Div. ASCE, 85, 67-94, 1959.

[49] Rosenbrock, H.H., Some General Implicit Processes for the Numerical Solution of Differential Equations, Computer J., 18, 50-64, 1964.

[50] Mavroeidis, G.P., Dong, G., Papageorgiou, A.S., Near-Fault Ground Motions, and the Response of Elastic and Inelastic Single-Degree-of-Freedom (SDOF) Systems. Earthq. Eng. Struct. Dyn., 33(9), 1023-49, 2004.

[51] Yadav, K.K., Gupta, V.K., Near-Fault Fling-Step Ground Motions: Characteristics and Simulation. Soil Dyn. Earthq. Eng., 101, 90-104, 2017.

[52] Bertero, V.V., Mahin, S.A., Herrera, R.A., Aseismic Design Implications of Near-Fault San Fernando Earthquake Records. Earthq. Eng. Struct. Dyn., 6(1), 31-42, 1978.

[53] Mavroeidis, G.P., Papageorgiou, A.S., A Mathematical Representation of Near-Fault Ground Motions. Bull. Seismol. Soc. Am., 93(3), 1099-131, 2003.

[54] Güler, E., Alhan, C., Effectiveness of Non-Linear Fluid Viscous Dampers in Seismically Isolated Buildings. Earthq. Struct., 17(2), 191-204, 2019.

[55] Hall, J.F., Heaton, T.H., Halling, M.W., Wald, D.J., Near-Source Ground Motion and its Effects on Flexible Buildings. Earthq. Spectra, 11(4), 569-605, 1995.

[56] Heaton, T.H., Hall, J.F., Wald, D.J., Halling, M.W., Response of High-Rise and Base-Isolated Buildings to a Hypothetical Mw 7.0 Blind Thrust Earthquake. Science, 267, 206-11, 1995.

[57] PEER, Pacific Earthquake Engineering Research Center Ground Motion Database, University of California, Berkeley, CA, 2013 (http://ngawest2.berkeley.edu).

[58] Saha, S.K., Matsagar, V.A., Jain, A.K., Response of Base-Isolated Liquid Storage Tanks under Near-Fault Earthquakes. Indian Society of Earthquake Technology Golden Jubilee Symposium, Roorkee, India, D011, 2012.

[59] Haroun, M.A., Vibration Studies and Tests of Liquid Storage Tanks. Earthq. Eng. Struct. Dyn., 11, 179-206, 1983.

[60] Malhotra, P.K., Method for Seismic Base Isolation of Liquid-Storage Tanks. J. Struct. Eng., 123, 113-6, 1997.

[61] Veletsos, A.S., Yang, J.Y., Earthquake Response of Liquid Storage Tanks. 2nd Engineering Mechanics Specialty Conference, ASCE, Raleigh, North Carolina, USA, pp. 1-24, 1977.